



# Electrochemical and spectroscopic properties of 1:2 Ni complexes of 1,3-substitued (CH<sub>3</sub>, OCH<sub>3</sub>) phenyl-5-phenylformazans

Habibe Tezcan\*, Elif Uzluk, Mehmet Levent Aksu

Department of Chemistry, Gazi University, Faculty of Gazi Education, Teknikokullar, 06500 Ankara, Turkey

## ARTICLE INFO

### Article history:

Received 26 October 2007

Received in revised form 5 February 2008

Accepted 9 February 2008

Available online 10 March 2008

### Keywords:

Formazan nickel(II) complexes

Platinum electrodes

Cyclic voltammetry

Oxidation mechanism

Spectroscopy

Substituent effect

## ABSTRACT

In this study, new 1:2 nickel complexes of 1-[*o*-, *m*-, *p*-(methyl, methoxyphenyl)]-3-(*p*-methoxyphenyl)-5-phenylformazans were synthesized. Their structures were elucidated and spectral behaviors were investigated with the use of elemental analysis, GC–mass, <sup>1</sup>H NMR, <sup>13</sup>C NMR, IR, and UV–vis spectra. The redox characteristics of these compounds have been investigated in nonaqueous dimethylsulfoxide at platinum and ultramicro platinum (10 μm) electrodes. Through controlled potential electrolysis, the oxidation products of each class of compounds can be separated and identified. The oxidation mechanism is suggested and it is proved. It was observed the oxidation mechanism take place in a single step two-electron or one-electron transfer to a disproportionation or dimerization reactions following the radical formation step. Eventually the relation between their absorption properties and electrochemical properties was examined.

© 2008 Elsevier Ltd. All rights reserved.

## 1. Introduction

Derivatives of formazans were synthesized and structural features, tautomeric and photochromic isomers were investigated [1–4]. Metal complexes of formazans were synthesized and structural determination, magnetic properties, complex stability constant determination and spectroscopic characterization and the formation of Fe complexes depending upon the pH value were investigated [5–11].

Formazans form tetrazolium salt when they are oxidized [12]. Tetrazolium salts are reduced back to formazans by the enzymes in the cell and stain the tissue. Tetrazolium–formazan system is classified as a marker of vitality and this feature enabled the determination of activity on tumor cell [13,14]. This feature caused an increasing interest in the chemistry and especially electrochemistry of formazans.

The study related to the redox behavior of formazans was carried out and it was claimed that ditetrazolium salts are reduced to both mono- and diformazans by one-electron transfer. The first one-electron transfer results in the formation of a tetrazolium radical and this radical was undergoing the disproportionation reaction [15]. Formazans are oxidized in a single step two-electron transfer followed by a deprotonation reaction forming corresponding tetrazolium cation [16].

As seen, many studies have been worked with formazans. But electrochemical studies of their nickel(II) complexes have not been reported in the literature. In this study, seven different formazan and their nickel(II) complexes of formazans have been synthesized (Scheme 1). Their structures were elucidated by elemental analyses, GC–mass, FTIR, and their spectral behaviors were investigated using <sup>1</sup>H NMR, <sup>13</sup>C NMR, FTIR and UV–vis spectral data. The effect of substituents on λ<sub>max</sub> values was determined.

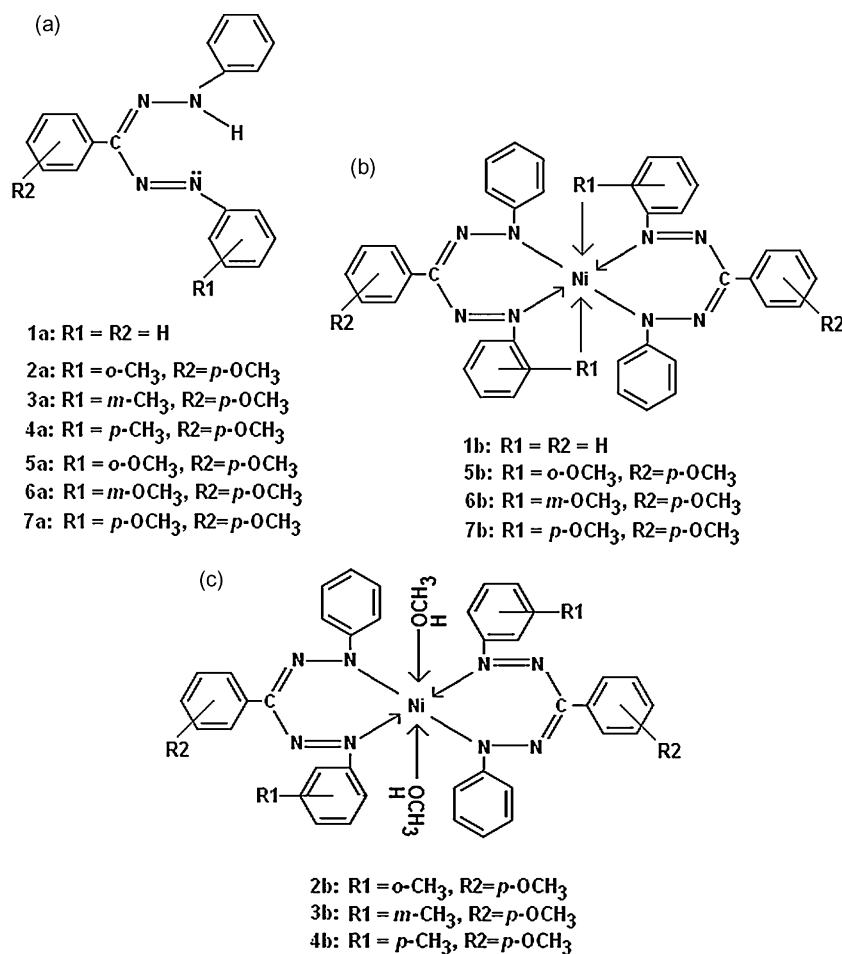
The biological activity of formazan makes the knowledge of its oxidation potentials and possible mechanisms are very important. Furthermore in this study is determined peak potentials (*E*<sub>ox</sub> and *E*<sub>red</sub>), diffusion coefficient (*D*), number of electrons transferred (*n*) and heterogeneous rate constant (*k*<sub>s</sub>) with the use of cyclic voltammetry, linear sweep voltammetry and chronoamperometry. Separation and identification of the intermediates and the final products were made through controlled potential electrolysis (CPE). A mechanistic scheme for the oxidation of formazan to tetrazolium salt was proposed based upon these data (Scheme 3).

## 2. Experimental

### 2.1. Reagents

All chemicals were obtained from Merck and Fluka except sodium hydroxide and [Ni(CH<sub>3</sub>COO)<sub>2</sub>·4H<sub>2</sub>O] that were purchased from Sigma–Aldrich. Deionized water (Millipore, Milli-Q) was used for synthesis; the organic solvents: CH<sub>3</sub>OH, CH<sub>3</sub>COCH<sub>3</sub>, dimethylsulfoxide (DMSO, 99.9%) and 1,4-dioxane were used for

\* Corresponding author. Tel.: +90 312 2021108; fax: +90 312 2227037.  
E-mail address: [habibe@gazi.edu.tr](mailto:habibe@gazi.edu.tr) (H. Tezcan).



**Scheme 1.** The structure of the formazans and their nickel(II) complexes synthesized.

electrochemical and spectroscopic measurements. Dimethylsulfoxide was used as solvent. During the solvent purification, all the processes were performed under a dry oxygen-free argon atmosphere. Fractionation was carried out using a 120 cm column filled with glass spirals at a recoil ratio 50:1. Purified solvent was stored under argon in the dark. DMSO (Merck) was boiled four times with calcium hydride (Merck) for 14 h (5 g/L) and subsequently fractionated at 14 Torr. Finally, the main fraction was carefully fractionated.

## 2.2. Measurements

The UV–vis spectra of the formazans synthesized in this study were obtained with UNICAM UV2-100 UV–visible spectrophotometer using 1 cm quartz cells in  $10^{-5}$  mol L<sup>-1</sup> DMSO and 325 nm lamps in the range of 250–600 nm. IR spectra were recorded on a MATT-SON 100-FTIR spectrophotometer between 4000 and 400 cm<sup>-1</sup> using KBr pellets. <sup>1</sup>H NMR spectra were performed on a Bruker AVANCE DPX-400 MHz and <sup>13</sup>C NMR 100 MHz spectrophotometer using CDCl<sub>3</sub> and *d*<sub>6</sub>-DMSO,  $10^{-4}$  mol L<sup>-1</sup>. Electrochemical studies were carried out with a computerized CHI Instrument 660 B system in a conventional three-electrode cell. A platinum electrode (PE) (CHI102) and a 10 μm-platinum ultramicrodisc electrode (UME) (CHI107) were used as a working electrode. The electrodes were cleaned by electrochemical potential cycling and washed with excess dimethylsulfoxide. A platinum wire was used as the auxiliary electrode. The reference electrode was a silver wire in constant contact with 0.1 M AgNO<sub>3</sub> in dimethylsulfoxide. Ferrocene (Fc) was used as an internal standard to measure formal

potential  $E^0$  vs. Fc<sup>0</sup>/Fc<sup>+</sup>. All measurements were carried out with  $1 \times 10^{-5}$  mol of the reactant in 10 mL dry oxygen-free solvent with 0.1 mol dm<sup>-3</sup> tetrabutylammonium tetrafluoroborate (TBA<sup>+</sup>BF<sub>4</sub><sup>-</sup>) as supporting electrolyte. All solutions were deaerated for 10 min with pure argon. All the measurements were taken at room temperature, 25 °C. The voltage scan rate range during the CV measurements was 10–10,000 mV/s. Elemental analyses were carried out using a LECO-CHNS-932 elemental analyser. Mass spectra were recorded on an AGILENT 1100 MSD mass spectrometer.

## 2.3. Controlled potential electrolysis (CPE)

CPE experiments were carried out in dry dimethylsulfoxide containing 0.1 mol dm<sup>-3</sup> tetrabutylammonium tetrafluoroborate (TBA<sup>+</sup>BF<sub>4</sub><sup>-</sup>) as supporting electrolyte. Compounds **1b** and **7b** are reported here as examples. The potential was controlled at the current plateau of the oxidation wave. As working electrode, a platinum electrode was used. The progress of the electrolysis was followed by recording periodically the decrease in current with time. From time to time the anode was removed from the cell, sprayed with pure acetone and burned in a direct flame, cooled and replaced in the cell. After the electrolysis was completed, the cell was disconnected from the circuit and the solvent was evaporated in vacuum. The residue was shaken with dry ether and the supporting electrolyte was filtered off.

The ethereal layer was evaporated in turn. The obtained residue was chromatographed on thin layer silica gel plates using chloroform as an eluent.

The main oxidation product obtained was scraped off the plate and extracted with dimethylsulfoxide, filtered and evaporated in vacuum.

#### 2.4. Synthesis of formazans

##### 2.4.1. 1,3,5-Triphenylformazan (**1a**)

1,3,5-Triphenylformazan was synthesized by the reaction of benzaldehyde (1.06 g, 0.01 mol), phenylhydrazine (1.08 g, 0.01 mol), aniline (0.93 g, 0.01 mol), concentrated HCl (5 mL) and sodium nitrite (0.75 g) in a methanol, at 0–5 °C alike literature [3,4]. Cherry red colored crystals: mp 172–173 °C; yield 78%. IR: 3069 cm<sup>-1</sup> (aromatic C–H), 3050–3000 cm<sup>-1</sup> (N–H), 1600 cm<sup>-1</sup> (aromatic C=C), 1500 cm<sup>-1</sup> (C=N), 1450 cm<sup>-1</sup> (N=N), 930–905 cm<sup>-1</sup> (CNNC). <sup>1</sup>H NMR: 8.32–7.27 ppm (15H, aromatic H), 1.18 ppm (1H, azo H). <sup>13</sup>C NMR: 148.80 ppm [1C, (imino-C) C=N], 141.98–119.54 ppm (8C, other carbons). Elemental analysis: calcd. for C<sub>19</sub>H<sub>16</sub>N<sub>4</sub>: C, 76.00; H, 5.33; N, 18.66. Found: C, 75.97; H, 5.29; N, 18.69%. Calcd. M: 300; found mass: *m/z* (eV) 301.10, 273.10, 223.00, 195.10, 105.05.

##### 2.4.2. 1-(*o*-, *m*-, *p*-Tolylphenyl)-3-(*p*-methoxyphenyl)-5-phenylformazans (**2a–4a**)

**2a–4a** were synthesized by the reaction of *p*-methoxybenzaldehyde (1.35 g, 0.01 mol), phenylhydrazine (1.08 g, 0.01 mol), *o*-, *m*-, *p*-tolylaniline (1.07 g, 0.01 mol), concentrated HCl (5 mL) and sodium nitrite (0.75 g) in a methanol, at 0–5 °C a method similar to that for 1,3,5-triphenylformazan. Each compound was recrystallized from methanol.

##### 2.4.3. Selected data for **2a**

Red-pink colored crystals: mp 187–188 °C; yield 69%. IR: 3480–3400 cm<sup>-1</sup> (aromatic C–H), 2920–2800 cm<sup>-1</sup> (N–H), 1600 cm<sup>-1</sup> (aromatic C=C), 1500 cm<sup>-1</sup> (C=N), 1220 cm<sup>-1</sup> (CH<sub>3</sub>), 1030 cm<sup>-1</sup> (N=N), 800–620 cm<sup>-1</sup> (CNNC). <sup>1</sup>H NMR: 8.21–6.97 ppm (13H, aromatic H), 1.60 ppm (1H, azo H), 2.56 ppm (3H, CH<sub>3</sub>), 3.90 ppm (3H, OCH<sub>3</sub>). <sup>13</sup>C NMR: 160.46 ppm [1C, (imino-C) C=N], 149.93–23.42 ppm (16C, other carbons). Elemental analysis: calcd. for C<sub>21</sub>H<sub>20</sub>N<sub>4</sub>O<sub>2</sub> (**2a**): C, 73.25; H, 5.81; N, 16.28. Found: C, 73.21; H, 5.76; N, 16.24%. Calcd M: 344.00; found mass: *m/z* (eV): 345.10, 239.10, 225.00, 119.00.

##### 2.4.4. Selected data for **3a**

Purple-red colored crystals: mp 210–211 °C; yield 40%. IR: 3490 cm<sup>-1</sup> (aromatic C–H), 3020–3010 cm<sup>-1</sup> (N–H), 1620 cm<sup>-1</sup> (aromatic C=C), 1495 cm<sup>-1</sup> (C=N), 1200 cm<sup>-1</sup> (CH<sub>3</sub>), 1020 cm<sup>-1</sup> (N=N), 850–600 cm<sup>-1</sup> (CNNC). <sup>1</sup>H NMR: 8.34–6.40 ppm (13H, aromatic H), 1.30 ppm (1H, azo H), 2.44 ppm (3H, CH<sub>3</sub>), 3.88 ppm (3H, OCH<sub>3</sub>). <sup>13</sup>C NMR: 160.80 ppm [1C, (imino-C) C=N], 147.36–22.80 ppm (16C, other carbons). Elemental analysis: calcd. for C<sub>21</sub>H<sub>20</sub>N<sub>4</sub>O<sub>2</sub> (**3a**): C, 73.25; H, 5.81; N, 16.28. Found: C, 73.19; H, 5.85; N, 16.34%. Calcd M: 344.00; found mass: *m/z* (eV): 345.50, 240.10, 226.00, 120.05.

##### 2.4.5. Selected data for **4a**

Dark purple colored crystals: mp 242–243 °C; yield 74%. IR: 3450–3440 cm<sup>-1</sup> (aromatic C–H), 2950–2820 cm<sup>-1</sup> (N–H), 1600 cm<sup>-1</sup> (aromatic C=C), 1500 cm<sup>-1</sup> (C=N), 1250 cm<sup>-1</sup> (CH<sub>3</sub>), 1010 cm<sup>-1</sup> (N=N), 840–540 cm<sup>-1</sup> (CNNC). <sup>1</sup>H NMR: 8.16–6.78 ppm (13H, aromatic H), 1.58 ppm (1H, azo H), 2.45 ppm (3H, CH<sub>3</sub>), 3.90 ppm (3H, OCH<sub>3</sub>). <sup>13</sup>C NMR: 160.39 ppm [1C, (imino-C) C=N], 148.88–21.56 ppm (14C, other carbons). Elemental analysis: calcd. for C<sub>21</sub>H<sub>20</sub>N<sub>4</sub>O<sub>2</sub> (**4a**): C, 73.25; H, 5.81; N, 16.28. Found: C, 73.28; H, 5.82; N, 16.20%. Calcd M: 344.00; found mass: *m/z* (eV): 345.05, 240.10, 226.50, 119.95.

##### 2.4.6. 1-(*o*-, *m*-, *p*-Methoxyphenyl)-3-(*p*-methoxyphenyl)-5-phenylformazans (**5a–7a**)

**5a–7a** were synthesized by the reaction of *p*-methoxybenzaldehyde (1.35 g, 0.01 mol), phenylhydrazine (1.08 g, 0.01 mol), *o*-, *m*-, *p*-methoxyaniline (1.28 g, 0.01 mol), concentrated HCl (5 mL) and sodium nitrite (0.75 g) in methanol, at 0–5 °C a method similar to that for 1,3,5-triphenylformazan. Each compound was recrystallized from methanol.

##### 2.4.7. Selected data for **5a**

Dark purple colored crystals: mp 196–197 °C; yield 71%. IR: 3490–3400 cm<sup>-1</sup> (aromatic C–H), 2900–2800 cm<sup>-1</sup> (N–H), 1600 cm<sup>-1</sup> (aromatic C=C), 1510 cm<sup>-1</sup> (C=N), 1250 cm<sup>-1</sup> (CH<sub>3</sub>), 1250 cm<sup>-1</sup> (OCH<sub>3</sub>), 1020 cm<sup>-1</sup> (N=N), 800–610 cm<sup>-1</sup> (CNNC). <sup>1</sup>H NMR: 8.26–6.83 ppm (13H, aromatic H), 1.31 ppm (1H, azo H), 4.01, 3.96 ppm (6H, OCH<sub>3</sub>). <sup>13</sup>C NMR: 160.36 ppm [1C, (imino-C) C=N], 151.86–55.98 ppm (16C, other carbons). Elemental analysis: calcd. for C<sub>21</sub>H<sub>20</sub>N<sub>4</sub>O (**5a**): C, 70.00; H, 5.55; N, 15.55. Found: C, 70.06; H, 5.51; N, 15.62%. Calcd. M: 360.00; found mass: *m/z* (eV) 361.10, 255.10, 225.10, 122.10.

##### 2.4.8. Selected data for **6a**

Red dark-purple colored crystals: mp 205–206.5 °C; yield 42%. IR: 3490–3400 cm<sup>-1</sup> (aromatic C–H), 3030 cm<sup>-1</sup> (N–H), 1600 cm<sup>-1</sup> (aromatic C=C), 1505 cm<sup>-1</sup> (C=N), 1210 cm<sup>-1</sup> (CH<sub>3</sub>), 1210 cm<sup>-1</sup> (OCH<sub>3</sub>), 1030 cm<sup>-1</sup> (N=N), 810–580 cm<sup>-1</sup> (CNNC). <sup>1</sup>H NMR: 8.36–6.58 ppm (13H, aromatic H), 1.30 ppm (1H, azo H), 3.91, 3.84 ppm (6H, OCH<sub>3</sub>). <sup>13</sup>C NMR: 164.50 ppm [1C, (imino-C) C=N], 160.02–55.90 ppm (16C, other carbons). Elemental analysis: calcd. for C<sub>21</sub>H<sub>20</sub>N<sub>4</sub>O (**6a**): C, 70.00; H, 5.55; N, 15.55. Found: C, 70.10; H, 5.48; N, 15.70%. Calcd. M: 360.00; found mass: *m/z* (eV) 361.05, 255.05, 226.05, 123.10.

##### 2.4.9. Selected data for **7a**

Dark purple colored crystals: mp 187–188 °C; yield 72%. IR: 3490 cm<sup>-1</sup> (aromatic C–H), 3050–3000 cm<sup>-1</sup> (N–H), 1600 cm<sup>-1</sup> (aromatic C=C), 1495 cm<sup>-1</sup> (C=N), 1250 cm<sup>-1</sup> (CH<sub>3</sub>), 1250 cm<sup>-1</sup> (OCH<sub>3</sub>), 1080 cm<sup>-1</sup> (N=N), 810–510 cm<sup>-1</sup> (CNNC). <sup>1</sup>H NMR: 8.12–6.87 ppm (13H, aromatic H), 1.31 ppm (1H, azo H), 3.90, 3.82 ppm (6H, OCH<sub>3</sub>). <sup>13</sup>C NMR: 162.84 ppm [1C, (imino-C) C=N], 160.37–55.70 ppm (14C, other carbons). Elemental analysis: calcd. for C<sub>21</sub>H<sub>20</sub>N<sub>4</sub>O (**7a**): C, 70.00; H, 5.55; N, 15.55. Found: C, 69.88; H, 5.58; N, 15.57%. Calcd. M: 360.00; found mass: *m/z* (eV) 361.15, 256.05, 225.35, 122.00.

#### 2.5. Synthesis of nickel(II) complexes

##### 2.5.1. Bis(1,3,5-triphenyl formazanato)nickel(II) complexes (**1b**)

1,3,5-Triphenylformazan (**1a**) (1.500 g, 0.005 mol) obtained as outlined in literature [3] was dissolved in dioxane (20 mL). In another flask [Ni(CH<sub>3</sub>COO)<sub>2</sub>·4H<sub>2</sub>O] salt (0.0025 mol, 0.625 g) was dissolved in ethanol (22 mL) under reflux with constant stirring at 25 °C and formazan is added to it stirring with a glass rod in 1–2 min. There was a no color change or precipitation observed during this process. The mixture was stirred with a magnetic stirrer at 30–35 °C under reflux. The precipitation started after an hour and the color turned into orange from red after 2 h and brown after 3 h. The stirring process was continued for 8 h. The color remained brown. The mixture was kept in the cupboard for 4 days. The light-brown precipitate was filtered off and washed with 10 mL 0.5 M NaOH, water and methanol. The compound was dried in stove at 40 °C for 24 h and recrystallized from methanol. Light-brown colored crystals: mp 300 °C; yield 85%. IR: 3098–3028 cm<sup>-1</sup> (aromatic C–H), 2963 cm<sup>-1</sup> (Ni-ligand), 1600 cm<sup>-1</sup> (aromatic C=C), 1500 cm<sup>-1</sup> (C=N), 1410 cm<sup>-1</sup> (N=N),

780–550  $\text{cm}^{-1}$  (CNNC).  $^1\text{H}$  NMR: 8.02–7.28 ppm (30H, aromatic H), 3.72–1.58 ppm [3H, solvent ( $\text{CH}_3\text{OH}$ )].  $^{13}\text{C}$  NMR: 174.81 ppm [1C, (imino-C) C=N], 163.97–118.50 ppm (17C, other carbons).

#### 2.5.2. Bis [1-(*o*-,*m*-,*p*-tolylphenyl)-3-(*p*-methoxyphenyl)-5-phenylformazanato]nickel(II) complexes (**2b–4b**)

**2a–4a** (0.690 g, 0.002 mol) obtained in Section 2.3 were dissolved in dioxane (15 mL). In another flask  $[\text{Ni}(\text{CH}_3\text{COO})_2 \cdot 4\text{H}_2\text{O}]$  (0.001 mol, 0.250 g) salt was dissolved in ethanol (15 mL) and formazans solution was added to it. The mixtures were stirred at 30–35 °C under reflux for 8 h. The resulting precipitates were kept in the cupboard for 3 days. Following the procedure outlined for compound **1b**. Each product was recrystallized from methanol.

#### 2.5.3. Selected data for **2b**

Light green-brown colored crystals: mp 244–245 °C; yield 69%. IR: 3480–3410  $\text{cm}^{-1}$  (aromatic C–H), 2937  $\text{cm}^{-1}$  (Ni-ligand), 1580  $\text{cm}^{-1}$  (aromatic C=C), 1518  $\text{cm}^{-1}$  (C=N), 1241  $\text{cm}^{-1}$  ( $\text{CH}_3$ ), 1027  $\text{cm}^{-1}$  (N=N), 839–589  $\text{cm}^{-1}$  (CNNC).  $^1\text{H}$  NMR: 8.23–6.92 ppm (26H, aromatic H), 2.50 ppm (6H,  $\text{CH}_3$ ), 3.90 ppm (6H,  $\text{OCH}_3$ ), 3.82, 1.22 ppm (2H,  $\text{CH}_3\text{OH}$ ).  $^{13}\text{C}$  NMR: 186.87 ppm [1C, (imino-C) C=N], 175.28–114.73 ppm (29C, other carbons). Elemental analysis calcd. for  $\text{NiC}_{42}\text{H}_{38}\text{N}_8\text{O}_2$  (**2b**): C, 64.89; H, 4.89; N, 14.42. Found: C, 64.93; H, 4.87; N, 14.47%. M: 744.70. Mass:  $m/z$  (eV), found: M.: 745.00. Other peaks: 418.05, 360.00, 226.05.

#### 2.5.4. Selected data for **3b**

Orange-brown colored crystals: mp 238 °C; yield 63%. IR: 3475–3410  $\text{cm}^{-1}$  (aromatic C–H), 2950  $\text{cm}^{-1}$  (Ni-ligand), 1580  $\text{cm}^{-1}$  (aromatic C=C), 1500  $\text{cm}^{-1}$  (C=N), 1241  $\text{cm}^{-1}$  ( $\text{CH}_3$ ), 1027  $\text{cm}^{-1}$  (N=N), 840–590  $\text{cm}^{-1}$  (CNNC).  $^1\text{H}$  NMR: 8.45–6.83 ppm (26H, aromatic H), 2.45 ppm (6H,  $\text{CH}_3$ ), 3.80 ppm (6H,  $\text{OCH}_3$ ), 3.83, 1.22 ppm (2H,  $\text{CH}_3\text{OH}$ ).  $^{13}\text{C}$  NMR: 185.87 ppm [1C, (imino-C) C=N], 177.60–117.05 ppm (29C, other carbons). Elemental analysis calcd. for  $\text{NiC}_{42}\text{H}_{38}\text{N}_8\text{O}_2$  (**3b**): C, 64.89; H, 4.89; N, 14.42. Found: C, 64.85; H, 4.95; N, 14.35%. M: 744.70. Mass:  $m/z$  (eV), found M: 744.80. Other peaks: 419.15, 359.10, 225.00.

#### 2.5.5. Selected data for **4b**

Light green-brown colored crystals: mp 295 °C; yield 61%. IR: 3450–3440  $\text{cm}^{-1}$  (aromatic C–H), 3062  $\text{cm}^{-1}$  (Ni-ligand), 2950–2820  $\text{cm}^{-1}$  (N–H), 1600  $\text{cm}^{-1}$  (aromatic C=C), 1500  $\text{cm}^{-1}$  (C=N), 1250  $\text{cm}^{-1}$  ( $\text{CH}_3$ ), 1010  $\text{cm}^{-1}$  (N=N).  $^1\text{H}$  NMR: 8.15–6.38 ppm (13H, aromatic H), 2.50 ppm (6H,  $\text{CH}_3$ ), 3.70 ppm (6H,  $\text{OCH}_3$ ), 3.74, 1.39 ppm (2H,  $\text{CH}_3\text{OH}$ ).  $^{13}\text{C}$  NMR: 174.80 ppm [1C, (imino-C) C=N], 169.11–118.21 ppm (25C, other carbons). Elemental analysis calcd. for  $\text{NiC}_{42}\text{H}_{38}\text{N}_8\text{O}_2$  (**4b**): C, 64.89; H, 4.89; N, 14.42. Found: C, 64.79; H, 4.83; N, 14.33%. M: 744.70. Mass:  $m/z$  (eV), found M: 745.10. Other peaks: 419.50, 359.10, 225.15.

#### 2.5.6. Bis [1-(*o*-,*m*-,*p*-methoxyphenyl)-3-(*p*-methoxyphenyl)-5-phenylformazanato]nickel(II) complexes (**5b–7b**)

**5a–7a** (0.690 g, 0.002 mol) prepared in Section 2.3 were dissolved in dioxane (15 mL) in another flask  $[\text{Ni}(\text{CH}_3\text{COO})_2 \cdot 4\text{H}_2\text{O}]$  (0.001 mol, 0.250 g) salt was dissolved in ethanol (15 mL) and formazans were added to it. Following the procedure outlined for compound **1b**. Each product was recrystallized from methanol.

#### 2.5.7. Selected data for **5b**

Pink-brown colored crystals: mp 225–226.5 °C; yield 73%. IR: 3490–3455  $\text{cm}^{-1}$  (aromatic C–H), 2964  $\text{cm}^{-1}$  (Ni-ligand), 1607  $\text{cm}^{-1}$  (aromatic C=C), 1509  $\text{cm}^{-1}$  (C=N), 1223  $\text{cm}^{-1}$  ( $\text{CH}_3$ ), 1027  $\text{cm}^{-1}$  (N=N), 839–616  $\text{cm}^{-1}$  (CNNC).  $^1\text{H}$  NMR: 8.28–6.41 ppm (26H, aromatic H), 4.02 ppm (12H,  $\text{OCH}_3$ ).  $^{13}\text{C}$  NMR: 186.87 ppm

[1C, (imino-C) C=N], 175.02–115.00 ppm (29C, other carbons). Elemental analysis calcd. for  $\text{NiC}_{42}\text{H}_{38}\text{N}_8\text{O}_4$  (**5b**): C, 70.72; H, 5.33; N, 15.71. Found: C, 70.78; H, 5.20; N, 15.76%. M.: 776.70. Mass:  $m/z$  (eV), found M.: 777.10. Other peaks: 402.00, 344.85, 226.10.

#### 2.5.8. Selected data for **6b**

Green colored crystals: mp 273 °C; yield 64%. IR: 3480–3420  $\text{cm}^{-1}$  (aromatic C–H), 2980  $\text{cm}^{-1}$  (Ni-ligand), 1580  $\text{cm}^{-1}$  (aromatic C=C), 1500  $\text{cm}^{-1}$  (C=N), 1240  $\text{cm}^{-1}$  ( $\text{CH}_3$ ), 1027  $\text{cm}^{-1}$  (N=N), 835–620  $\text{cm}^{-1}$  (CNNC).  $^1\text{H}$  NMR: 8.42–6.80 ppm (26H, aromatic H), 3.92 ppm (12H,  $\text{OCH}_3$ ).  $^{13}\text{C}$  NMR: 185.56 ppm [1C, (imino-C) C=N], 177.42–113.32 ppm (29C, other carbons). Elemental analysis calcd. for  $\text{NiC}_{42}\text{H}_{38}\text{N}_8\text{O}_4$  (**6b**): C, 70.72; H, 5.33; N, 15.71. Found: C, 70.65; H, 5.28; N, 15.67%. M.: 776.70. Mass:  $m/z$  (eV), found M: 777.03. Other peaks: 401.80, 345.20, 225.10.

#### 2.5.9. Selected data for **7b**

Green colored crystals: mp 271–272 °C; yield 60%. IR: 3450–3440  $\text{cm}^{-1}$  (aromatic C–H), 3058  $\text{cm}^{-1}$  (Ni-ligand), 2950–2820  $\text{cm}^{-1}$  (N–H), 1600  $\text{cm}^{-1}$  (aromatic C=C), 1500  $\text{cm}^{-1}$  (C=N), 1250  $\text{cm}^{-1}$  ( $\text{CH}_3$ ), 1010  $\text{cm}^{-1}$  (N=N).  $^1\text{H}$  NMR: 8.21–6.68 ppm (26H, aromatic H), 3.89 ppm (12H,  $\text{OCH}_3$ ).  $^{13}\text{C}$  NMR: 182.62 ppm [1C, (imino-C) C=N], 175.24–117.38 ppm (25C, other carbons). Elemental analysis calcd. for  $\text{NiC}_{42}\text{H}_{38}\text{N}_8\text{O}_4$  (**7b**): C, 70.72; H, 5.33; N, 15.71. Found: C, 70.80; H, 5.30; N, 15.78%. M.: 776.70. Mass:  $m/z$  (eV), found M: 777.50. Other peaks: 401.55, 345.65, 225.50.

All the synthesized compounds (**1a–7a**, **1b–7b**) were purified by repeated crystallization, dried under reduced pressure and the purity was checked by thin layer chromatography.

#### 2.6. Oxidation product of **1b**

Elemental analysis calculated: C, 76.25; H, 5.02; N, 18.73. Found: C, 76.80; H, 5.13; N, 18.57%. Mass:  $m/z$  (eV), calculated M: 598.00. Mass spectrum shows the main fragments at  $m/z$  599.10, parent 493.00; 388.00; 311.00; 234.00; 157.00.

#### 2.7. Oxidation product of **7b**

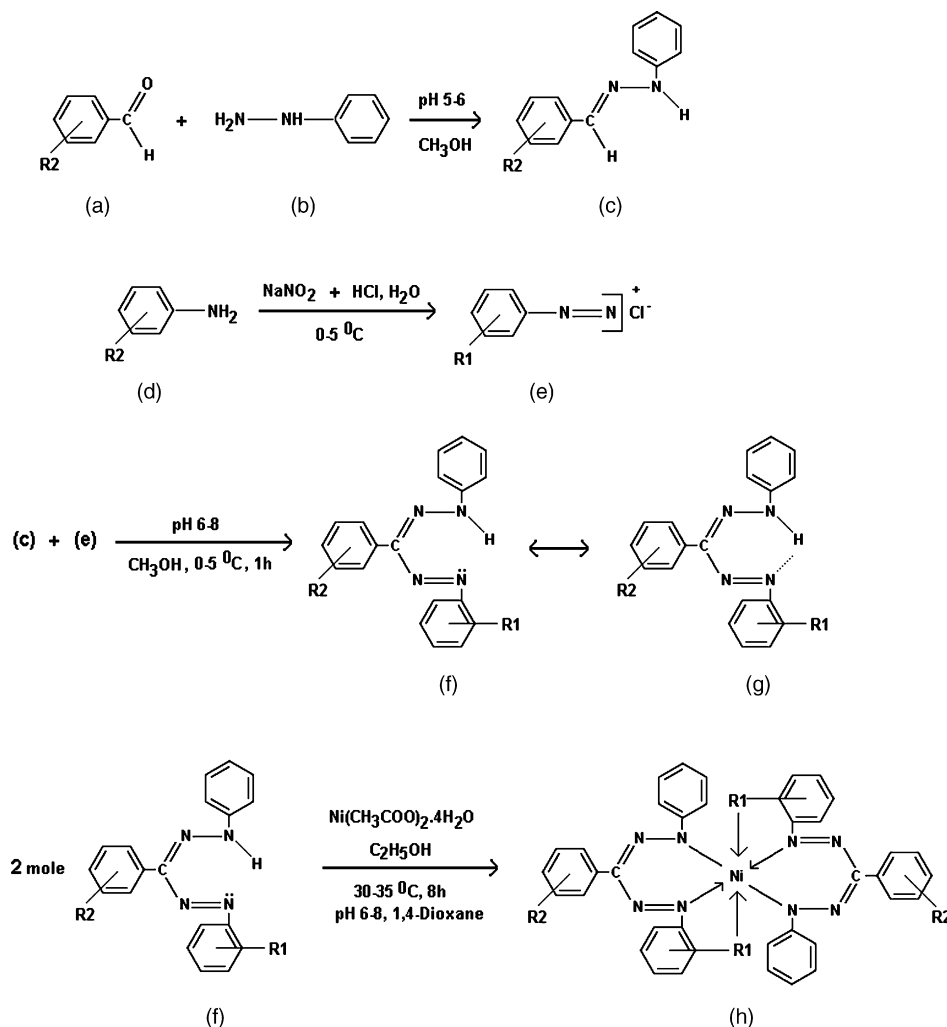
Elemental analysis calculated: C, 73.47; H, 5.54; N, 16.32. Found: C, 73.28; H, 5.49; N, 16.20%. Mass:  $m/z$  (eV), calculated M: 343.00. Mass spectrum shows the main fragments at  $m/z$  344.00, parent 224.00; 135.00; 131.00; 105.00.

### 3. Result and discussion

#### 3.1. Synthesis and spectral properties of formazans and their nickel(II) complexes

This study was carried out in four stages. In the first and two steps, formazans and their nickel(II) complexes were synthesized. In the third step, their structures were elucidated then spectroscopic features and the effect of substituents on the absorption properties of compounds were investigated. In the fourth step, electrochemical properties were investigated. The intermediate hydrazones (**c**) were synthesized at pH 5–6 and the syntheses of formazans were carried out at pH 9–12. Nickel(II) complexes of formazans were synthesized at pH 6–8 according to the literature [5] in order to prevent the formation of different isomers. The reaction scheme is given in Scheme 2.

Elemental analysis and mass spectroscopic data are corroborated the structures proposed in Scheme 1. When one examines  $^1\text{H}$  NMR data shows that the aromatic-H peak for Ni-TPF (**1b**) are observed at  $\delta = 8.02$ –7.28 ppm. In nickel(II) complexes of formazans



Scheme 2. Synthesis of formazans and their nickel(II) complexes.

**2b–4b; 5b–7b** where position of 3-phenyl ring is substituted with *p*-OCH<sub>3</sub> while –CH<sub>3</sub>, –OCH<sub>3</sub> is each substituted to *o*-, *m*-, *p*-positions of the 1-phenyl ring, the aromatic-H signals (8.23, 8.45 and 8.15 ppm; 8.28, 8.42 and 8.21 ppm, respectively) are shifted towards lower fields according to Ni-TPF (**1b**). There is a shift towards lower fields in the case of electron donating groups such as CH<sub>3</sub> and OCH<sub>3</sub> this is not at the same dimension with that of the electron withdrawing groups. This can be explained by the fact that the electron donating effects of CH<sub>3</sub> and OCH<sub>3</sub> can be neglected against the strong electron withdrawing effect of Ni<sup>2+</sup>. When aromatic-H peaks nickel(II) complexes are compared with the corresponding formazans they were observed to shift towards lower fields. This is in accordance with the fact that the electrons in the structure are withdrawn with the insertion of Ni<sup>2+</sup> into formazans structure [8,18,19]. N–H peak observed at 1.60–1.18 ppm in formazans disappeared in nickel(II) complexes. This is a further proof that metal ion was inserted in place of proton of N–H group. Also the peaks appeared at 3.90–1.22 ppm were attributed to the solvent (CH<sub>3</sub>OH). This was an expected outcome. These data are supported by the IR results.

The  $\delta$  values for the imino-C (C=N) carbon for Ni-TPF (**1b**) was observed at 174.81 ppm. The attachment of an electron donating group to the 1-phenyl ring such as CH<sub>3</sub> and OCH<sub>3</sub> caused the  $\delta$  values showed a slight increase. C=N carbon peaks of nickel(II)

complexes are in lower fields compared with those of corresponding formazans. While C=N peaks observed between 164.50 and 148.80 ppm in formazans are shifted to 186.87–174.80 ppm in nickel(II) complexes. This result is in accordance with the insertion of an electron withdrawing group Ni<sup>2+</sup> into the system. Other C peaks can also be evaluated in a similar manner [19].

The C=N stretching band of Ni-TPF (**1b**) was observed at 1500 cm<sup>-1</sup>. The band related to the *o*-, *m*-, *p*-substituted CH<sub>3</sub> (**2b–4b**) on the 1-phenyl ring were observed at 1518, 1500 and 1500 cm<sup>-1</sup>. These peaks appeared at 1509, 1500 and 1500 cm<sup>-1</sup> in the case of *o*-, *m*-, *p*-OCH<sub>3</sub> substitution (**5b–7b**). The C=N bands observed at 1510–1495 cm<sup>-1</sup> in formazans were observed to shift to 1518–1500 cm<sup>-1</sup> in nickel(II) complexes. The N–H band observed at 3050–2800 cm<sup>-1</sup> in formazans was observed to generally disappear in their nickel(II) complexes. However, new peaks observed at 3062–2937 cm<sup>-1</sup>. These peaks were attributed to metal–ligand bonds. This is the verification of the formation of nickel(II) complexes as a result of insertion of Ni<sup>2+</sup> in place of an H atom in N–H [7,20]. These results confirm the formula given in Scheme 1b–c. However, the N–H band were weakly observed in compounds **4b, 7b**. These results are in agreement with the literature [6]. N=N band observed at 1410 cm<sup>-1</sup> in Ni-TPF (**1b**) this bond was seen to shift to 1027 cm<sup>-1</sup> in *o*-, *m*-, *p*-CH<sub>3</sub> substituted nickel(II) complexes (**2b–4b**) and 1027, 1027 and 1054 cm<sup>-1</sup> *o*-, *m*-, *p*-OCH<sub>3</sub> substituted nickel(II)

**Table 1**  
UV–visible absorption maxima of the nickel(II) complexes formazans **1b–7b** (DMSO,  $10^{-5}$  mol/L)

Compound	$\lambda_{\max 1}$ (nm)	$\epsilon (\times 10^3 \text{ M}^{-1} \text{ cm}^{-1})$	$\lambda_{\max 2}$ (nm)	$\epsilon (\times 10^4 \text{ M}^{-1} \text{ cm}^{-1})$	$\lambda_{\max 3}$ (nm)	$\epsilon (\times 10^4 \text{ M}^{-1} \text{ cm}^{-1})$	Wavelength shift ( $\Delta\lambda_{\max}$ )
<b>1b</b>	611.0	6.78	448.0	5.00	275.0	7.80	–
<b>2b</b>	654.0	5.16	458.0	3.40	307.0	11.34	43
<b>3b</b>	647.0	5.76	454.0	4.70	299.0	11.20	36
<b>4b</b>	644.0	3.95	452.0	8.80	–	–	33
<b>5b</b>	661.0	3.12	460.0	3.76	311.0	15.60	50
<b>6b</b>	649.0	5.20	464.0	5.30	322.0	12.60	38
<b>7b</b>	642.0	3.67	456.0	1.80	274.0	13.92	31

Column 8:  $\Delta\lambda_{\max} = \lambda_{\max 1}$  (Ni-TPF),  $\lambda_{\max 1}$  (substituted nickel(II) complexes of formazans).

complexes (**5b–7b**) N=N band was observed to shift towards the lower frequencies in Ni-TPF (**1b**) complex than its respective formazan (**1a**). This band also shifted to lower frequencies in  $\text{CH}_3$  and  $\text{OCH}_3$  substituted formazans nickel(II) complexes compared to Ni-TPF (**1b**). The results are in agreement with the literature [7,20]. Other aromatic C–H, C=C and CNNC stretching peaks in the complexes and the peaks related to  $\text{CH}_3$ ,  $\text{OCH}_3$  in the corresponding compounds were observed in their expected region [20].

There were three peaks observed in the UV–vis spectra of nickel(II) complexes of formazans. The absorptions peaks  $\lambda_{\max 1}$  the nickel(II) complex,  $\lambda_{\max 2}$  formazan unit and  $\lambda_{\max 3}$  hydrazone unit were attributed [8]. The  $\lambda_{\max 1}$  observed at 482–531 nm in formazans shifted to 611–661 nm in their nickel(II) complexes (Table 1). This is in accordance with the fact that the electrons in the structure are withdrawn with the insertion of  $\text{Ni}^{2+}$  into complex structure. These results are in compliance with literature [5,6,8–11]. When  $\Delta\lambda_{\max}$  values are compared according to the type of the substituents it was observed that the amount of shift was higher when 1-pheny ring was attached with electron donating groups such as  $\text{CH}_3$  and  $\text{OCH}_3$ . These results are

depicted in Fig. 1a and b. In the complexes containing  $\text{CH}_3$  and  $\text{OCH}_3$  the amount of shifts observed in absorption values ( $\Delta\lambda_{\max}$ ) was observed to follow the order of  $o$ -> $m$ -> $p$ -. If we think that electron withdrawing effect results only from the inductive effect which diminishes as we move from the center this order is an expected outcome.

### 3.2. Cyclic voltammetry

The cyclic voltammetric behavior of the nickel(II) complexes of formazans were studied in anhydrous DMSO (dimethylsulfoxide) at room temperature. The cyclic voltammograms of substituted ( $-\text{CH}_3$  and  $-\text{OCH}_3$ ) nickel(II) complexes (**2b–7b**) are compared with the parent compound Ni-TPF (**1b**). Figs. 2–4 show a typical cyclic voltammograms of these compounds.

A cyclic voltammogram of Ni-TPF (**1**) is shown in Fig. 2. The scan showed one anodic wave and one cathodic wave. A cyclic sweep in the  $-1.60$  to  $+0.00$  V range shows an anodic peak at  $E_{\text{ox}1} = -1260.6$  mV and a cathodic peak at  $E_{\text{red}1} = -798.1$  mV. As seen from Fig. 2, Ni-TPF (**1b**) gives one-electron transfer. This complex probably gives dimerization or disproportionation reaction following the radical formation step at  $-1260.6$  mV. However, it seems that the substituted groups ( $-\text{CH}_3$  and  $-\text{OCH}_3$ ) have quite effect upon the electrochemical behavior of the nickel(II) complexes of formazans in Figs. 3 and 4.

As seen from Fig. 3 and Table 2, compounds **2b–4b** caused major changes in both the peak potential and the peak currents as compared with the parent Ni-TPF (**1b**).  $o$ - and  $p$ - $\text{CH}_3$  sub-

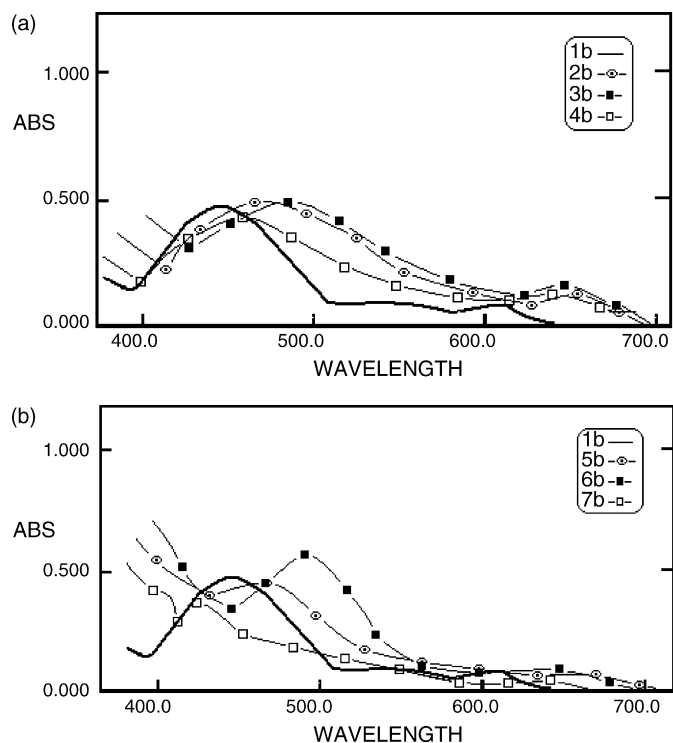


**Fig. 1.** Absorption spectra of (a)  $1.0 \times 10^{-5}$  M DMSO solutions of compounds **2b–4b** compared to Ni-TPF (**1b**); (b)  $1.0 \times 10^{-5}$  M DMSO solutions of compounds **5b–7b** compared to Ni-TPF (**1b**).

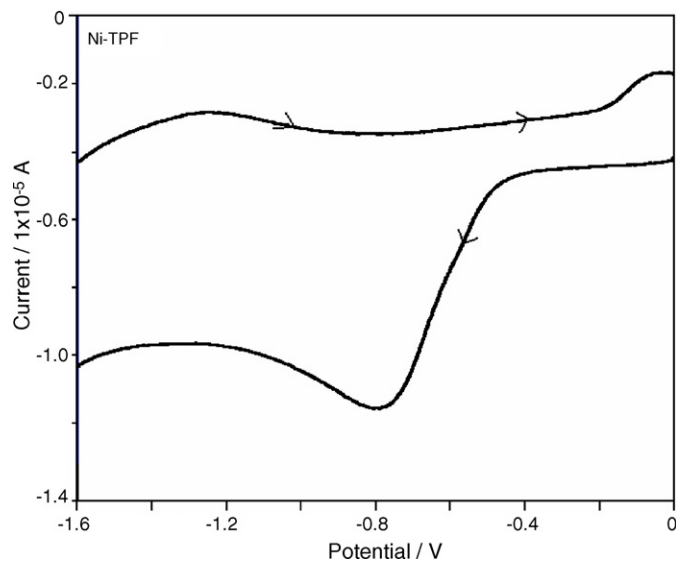


**Fig. 2.** Cyclic voltammogram of a DMSO solution of  $1.0 \times 10^{-5}$  M Ni-TPF (**1b**) in the presence of 0.1 M  $\text{TBA}^+\text{BF}_4^-$  at Pt electrode. Potential scan rate:  $100 \text{ mV s}^{-1}$ .

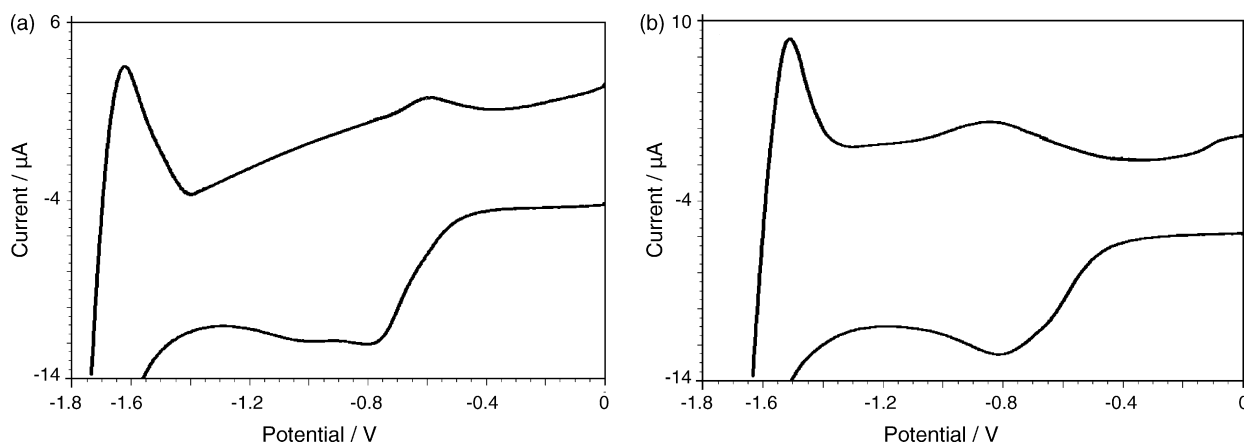


Fig. 3. Representative cyclic voltammogram in DMSO (25 °C, ionic strength, 0.1 M TBA<sup>+</sup>BF<sub>4</sub><sup>-</sup>;  $v$ , 100 mV s<sup>-1</sup>): (a)  $1.0 \times 10^{-5}$  M compound **2b** and (b)  $1.0 \times 10^{-5}$  M **4b**.

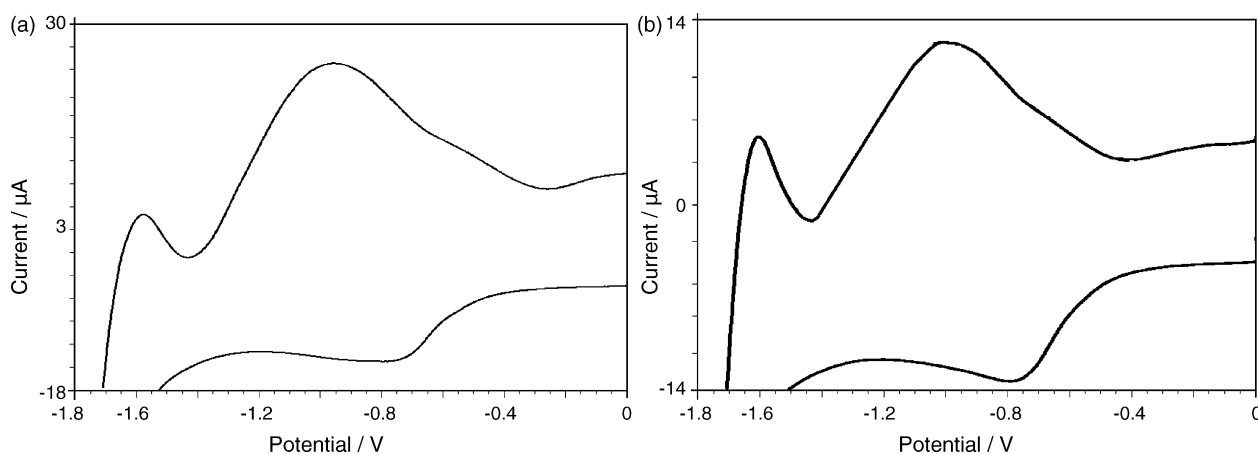


Fig. 4. Representative cyclic voltammogram in DMSO (25 °C, ionic strength, 0.1 M TBA<sup>+</sup>BF<sub>4</sub><sup>-</sup>;  $v$ , 100 mV s<sup>-1</sup>): (a) compound  $1.0 \times 10^{-5}$  M **5b** and (b)  $1.0 \times 10^{-5}$  M **7b**.

stituted nickel(II) complexes (**2b**, **4b**) directly give tetrazolium cations (TPT<sup>+</sup>) by a single step two-electron transfer. Compound **3b** behaves similarly towards oxidation; they are oxidized by one-electron process. This complex (**3b**) probably gives dimerization or disproportionation reaction following the radical formation step.

The scans of complexes **2b** and **4b** showed two anodic waves and one cathodic wave. On oxidation of  $-CH_3$  substituted nickel(II) complexes, oxidation peaks were observed more cathodic potential in the *o*-, *m*-, *p*-CH<sub>3</sub> (complexes **2b–4b**) compared with Ni-TPF (**1b**). A cyclic sweep in the  $-1.80$  to  $+0.00$  V range shows two anodic peaks at  $E_{ox1} = -1623.8$  mV,  $E_{ox2} = -590.4$  mV and a cathodic peak at  $E_{red1} = -807.4$  mV for compound **2b** (Fig. 3a). In the same range, two anodic peaks ( $E_{ox1}$  and  $E_{ox2}$ ) are appeared at  $-1510.6$  and  $-842.9$  mV, respectively. A cathodic peak ( $E_{red1}$ ) is observed at

$-814.6$  mV for compound **4b** (Fig. 3b). In the same range, an anodic peak ( $E_{ox1}$ ) is obtained at  $-1570.0$  mV and a cathodic peak ( $E_{red1}$ ) is observed at  $-840.0$  mV for compound **3b**. However, the intensities of the first peak ( $E_{ox1}$ ) for the complex **3b** are much higher compared with the *o*-CH<sub>3</sub> substituted nickel(II) complex (**2b**). This shows that the electron transfer rate is much lower in *o*-CH<sub>3</sub> substituted nickel(II) complex **2b**. The intensity of the first peak ( $E_{ox1}$ ) is much higher for the *p*-CH<sub>3</sub> substituted nickel(II) complex **4b** compared with those of *o*- and *m*-CH<sub>3</sub> substituted nickel(II) complexes. The intensity of the first peak changes as *p*->*m*->*o*-CH<sub>3</sub> substituted nickel(II) complexes. These results also are in accordance with the spectroscopic data.

As seen from Fig. 4 and Table 2, compounds **5b–7b** caused amount changes in both the peak potential and the peak currents as compared with the parent Ni-TPF (**1b**). *o*-, *m*-, *p*-OCH<sub>3</sub> substi-

Table 2  
Voltamperometric results of nickel(II) complexes (**1b–7b**)

Compound	$E_{ox1}$ (mV)	$I_{pox1}$ ( $\mu$ A)	$E_{ox2}$ (mV)	$I_{pox2}$ ( $\mu$ A)	$E_{red1}$ (mV)	$I_{pred1}$ ( $\mu$ A)	$\Delta E_p$ (mV)	$k_s$ (cm s <sup>-1</sup> )
<b>1b</b>	-1260.6	3.086	–	1.789	-798.1	2.657	-462.5	$11.964 \times 10^{-3}$
<b>2b</b>	-1623.8	3.445	-590.4	1.799	-807.4	12.070	-820.9	$1.714 \times 10^{-3}$
<b>3b</b>	-1570.0	6.260	–	–	-842.2	11.780	-727.8	$6.464 \times 10^{-3}$
<b>4b</b>	-1510.6	8.765	-842.9	3.280	-814.6	12.220	-696.0	$5.371 \times 10^{-3}$
<b>5b</b>	-1576.8	6.027	-956.2	24.880	-757.9	14.070	-818.9	$3.785 \times 10^{-3}$
<b>6b</b>	-1590.2	5.456	-795.7	20.879	-890.7	12.457	-699.5	$4.605 \times 10^{-3}$
<b>7b</b>	-1607.5	5.101	-1008.0	12.260	-795.6	14.044	-811.9	$2.298 \times 10^{-3}$

Column 8:  $\Delta E_p$ :  $E_{ox1} - E_{red1}$  (mV). Cyclic voltammograms were obtained in DMSO at 25 °C at platinum electrode, ionic strength 0.1 M (TBA<sup>+</sup>BF<sub>4</sub><sup>-</sup>), sweep speed: 100 mV s<sup>-1</sup>.  $E_{ox}$ : oxidation;  $E_{red}$ : reduction,  $k_s$ /cm s<sup>-1</sup> values.

**Table 3**  
Voltamperometric data of nickel(II) complexes (**1b–7b**) in DMSO at platinum electrode and 25°C, ionic strength 0.1 M (TBA<sup>+</sup>BF<sub>4</sub><sup>-</sup>), scan rates: 10, 1000 and 10,000 mV s<sup>-1</sup>

Comp	Scan rate (mV/s)	$E_{ox1}$ (mV)	$I_{pox1}$ ( $\mu$ A)	$E_{ox2}$ (mV)	$I_{pox2}$ ( $\mu$ A)	$E_{red1}$ (mV)	$I_{pred1}$ ( $\mu$ A)
<b>1b</b>	10	-1477.0	3.923	-	-	-803.5	5.287
	1,000	-1168.3	3.430	-	-	-900.5	23.110
	10,000	-1632.0	9.499	-	-	-1144.5	42.190
<b>2b</b>	10	-1656.5	3.367	-1091.8	4.268	-1053.6	9.599
	1,000	-1536.0	44.560	-1306.6	21.000	-1096.0	26.670
	10,000	-1005.0	68.990	-	-	-1094.6	87.490
<b>3b</b>	10	-1593.4	3.490	-	-	-875.9	6.239
	1,000	-1510.0	2.890	-	-	-789.0	17.890
	10,000	-1223.0	66.890	-	-	-1100.3	77.900
<b>4b</b>	10	-1530.0	2.792	-978.3	6.749	-863.4	8.667
	1,000	-1441.7	77.130	-	-	-847.7	32.740
	10,000	-1145.6	140.000	-	-	-941.7	100.700
<b>5b</b>	10	-1559.5	2.499	-936.0	1.299	-885.0	10.300
	1,000	-1515.4	63.760	-1215.4	27.820	-897.6	36.560
	10,000	-1171.8	103.800	-	-	-1077.5	122.500
<b>6b</b>	10	-1597.6	6.780	-	-	-895.6	9.100
	1,000	-1390.5	23.560	-	-	-810.0	43.240
	10,000	-1234.5	56.890	-	-	-978.6	89.100
<b>7b</b>	10	-1597.7	2.381	-1259.5	3.244	-953.5	8.306
	1,000	-1483.0	69.380	-1215.4	30.000	-862.3	32.820
	10,000	-1132.6	79.010	-	-	-986.2	95.010

$E_{ox}$ : oxidation;  $E_{red}$ : reduction.

**Table 4**  
Some of the parameters calculated for nickel(II) complexes (**1b–7b**)

Compound	C (mM)	$I_{ss}$ ( $\times 10^{-10}$ A)	Cottrell slope ( $S \times 10^{-5}$ )	$n$	$n$ net	$D$ ( $\times 10^{-6}$ cm <sup>2</sup> s <sup>-1</sup> )
<b>1b</b>	7.8	4.417	1.249	0.88	1	1.667
<b>2b</b>	8.1	2.056	1.182	1.63	2	0.330
<b>3b</b>	8.0	4.300	1.395	1.10	1	1.392
<b>4b</b>	7.9	4.610	1.863	1.85	2	0.755
<b>5b</b>	8.0	5.227	1.963	1.79	2	0.846
<b>6b</b>	8.1	6.040	2.096	1.74	2	0.966
<b>7b</b>	7.5	2.454	1.273	1.71	2	0.424

tuted nickel(II) complexes (**5b–7b**) directly give tetrazolium cations (TPT<sup>+</sup>) by a single step two-electron transfer.

At the oxidation peaks were observed more cathodic potential in the *o*-, *m*-, *p*-OCH<sub>3</sub> complexes **5b–7b** compared with Ni-TPF (**1b**).

The scans of compounds **5b–7b** showed two anodic waves and one cathodic wave. In the -1.80 to +0.00 V range, two anodic peaks ( $E_{ox1}$  and  $E_{ox2}$ ) are appeared at -1576.8 and -956.2 mV, respectively, and a cathodic peak ( $E_{red1}$ ) is observed at -757.9 mV

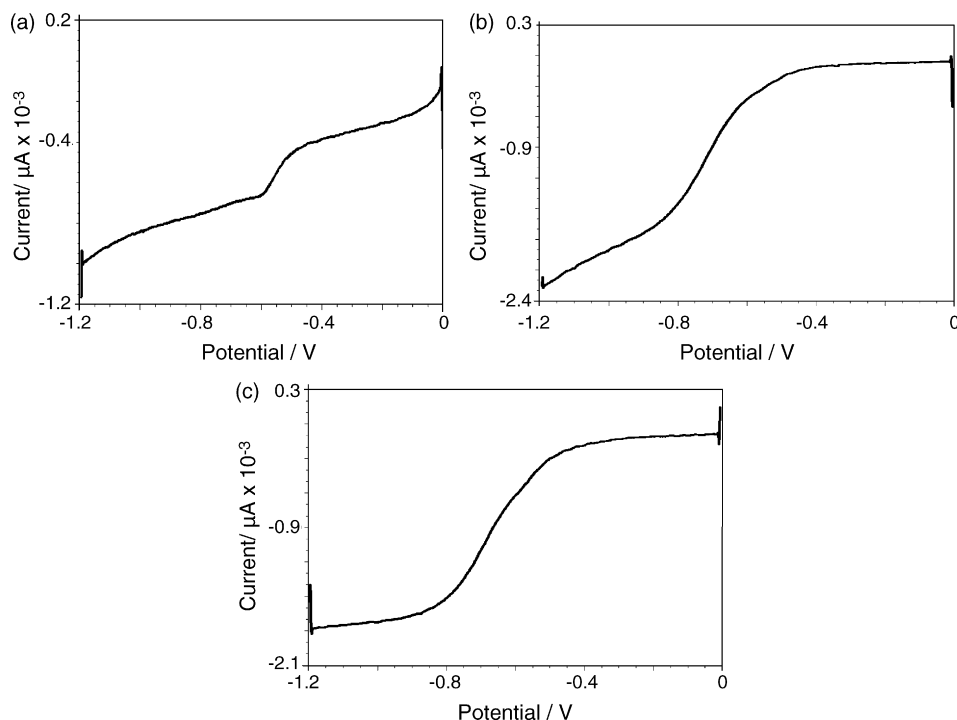


**Fig. 5.** UME curves of DMSO solutions of  $1.0 \times 10^{-5}$  M compounds Ni-TPF, **1b** (a); **2b** (b); **4b** in the presence of 0.1 M TBA<sup>+</sup>BF<sub>4</sub><sup>-</sup> at 10  $\mu$ m-platinum ultramicro electrode. Potential scan rate: 10 mV s<sup>-1</sup>.

for compound **5b** (Fig. 4a). In the same range, two anodic peaks at  $E_{ox1} = -1590.2$  mV,  $E_{ox2} = -795.7$  mV and a cathodic peak at  $E_{red1} = -890.7$  mV for compound **6b**. In the same range, two anodic peaks ( $E_{ox1}$  and  $E_{ox2}$ ) are appeared at  $-1607.5$  and  $-1008.0$  mV, respectively, and a cathodic peak ( $E_{red1}$ ) is observed at  $-795.6$  mV for compound **7b** (Fig. 4b). However, the intensities of the first peak ( $E_{ox1}$ ) for the complex **6b** is much lower compared with the *o*-OCH<sub>3</sub> substituted nickel(II) complex. This shows that the electron transfer rate is much lower in *o*-OCH<sub>3</sub> substituted nickel(II) complex. The intensity of the first peak ( $E_{ox1}$ ) is much lower for the *p*-OCH<sub>3</sub> substituted nickel(II) complex compared with those of *o*- and *m*-OCH<sub>3</sub> substituted nickel(II) complexes. This may be explained by the decreasing inductive effect going from *o*- to *p*-position. The intensity of the first peak changes as *o*->*m*->*p*-OCH<sub>3</sub> substituted nickel(II) complexes. This is in accordance with the yield of *p*-OCH<sub>3</sub> substituted nickel(II) complex was the highest followed by *m*-OCH<sub>3</sub> and *o*-OCH<sub>3</sub> substituted nickel(II) complexes. These results also are in accordance with the spectroscopic data. -OCH<sub>3</sub> group more cathodic potential was shifted according to -CH<sub>3</sub> group when substituents were compared each other. This result is agreement with -OCH<sub>3</sub> group is a stronger electron-donating group according to -CH<sub>3</sub> group.

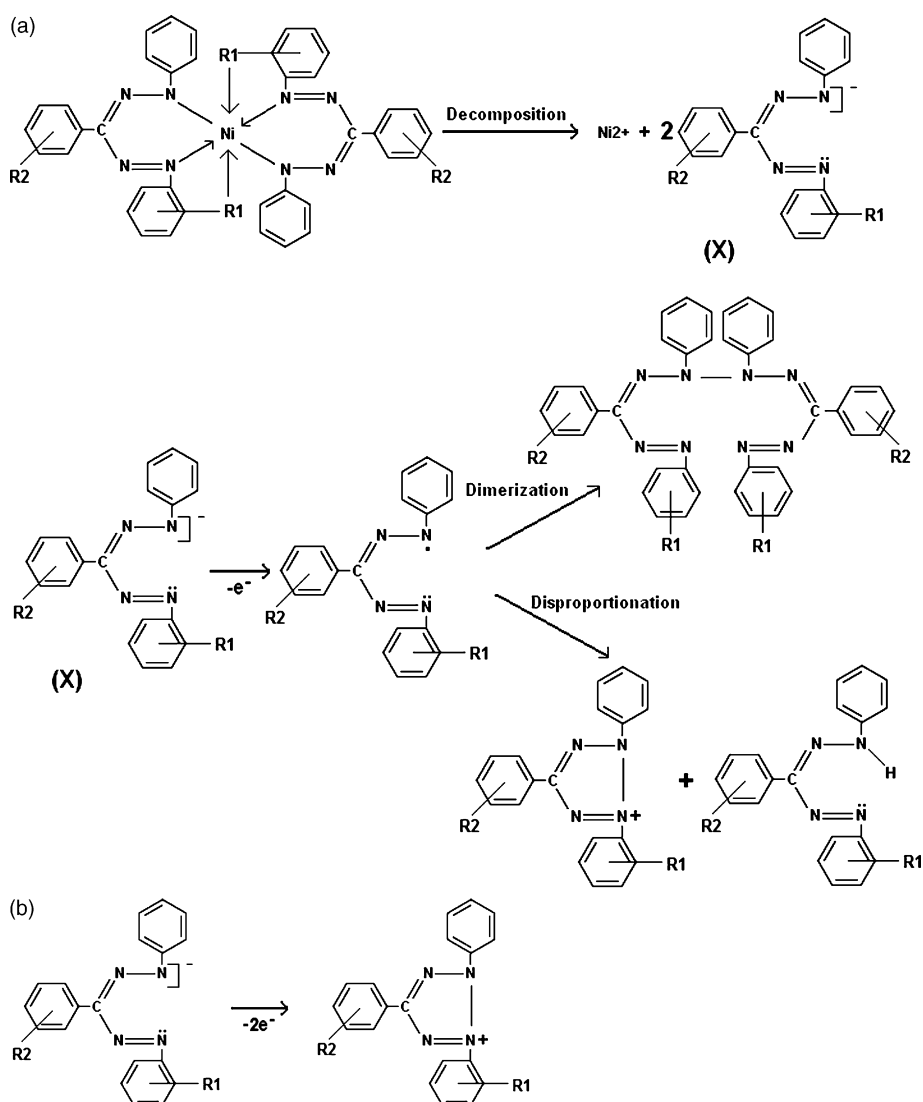
Consequently, peak potentials are dependent upon the type and position of substituents. All the cyclic voltammetric data are tabulated in Tables 2 and 3.

### 3.3. Linear sweep voltammetry and chronoamperometry

The number of electron transferred ( $n$ ) and the diffusion coefficients ( $D$ ) were determined by the ultramicroelectrode CV technique of Baranski et al. [17]. The diffusion coefficients ( $D$ ) of the compounds **1b–7b** were calculated from the Cottrell equation after the  $n$  values had been obtained. The  $D$  values are tabulated in Table 4. The number of electrons transferred was found to be in accordance with the CV data. The diffusion coefficients were also found within expected dimensions. The results of UME and chronoamperometric data are tabulated in Table 4.

#### 3.3.1. The calculation of the number of electrons transferred

The number of electrons transferred was obtained with the use of chronoamperometric Cottrell equation and ultramicro Pt disc electrode (UME) steady state current [17]. The real surface area of the Pt electrode was found to be 2.58 cm<sup>2</sup> with the use ferrocene.



**Scheme 3.** (a) Possible oxidation mechanism of compound **1b** (Ni-TPF) and compound **3b**. (b) Possible oxidation mechanism of compounds **2b**, **4b** and **5b–7b**.

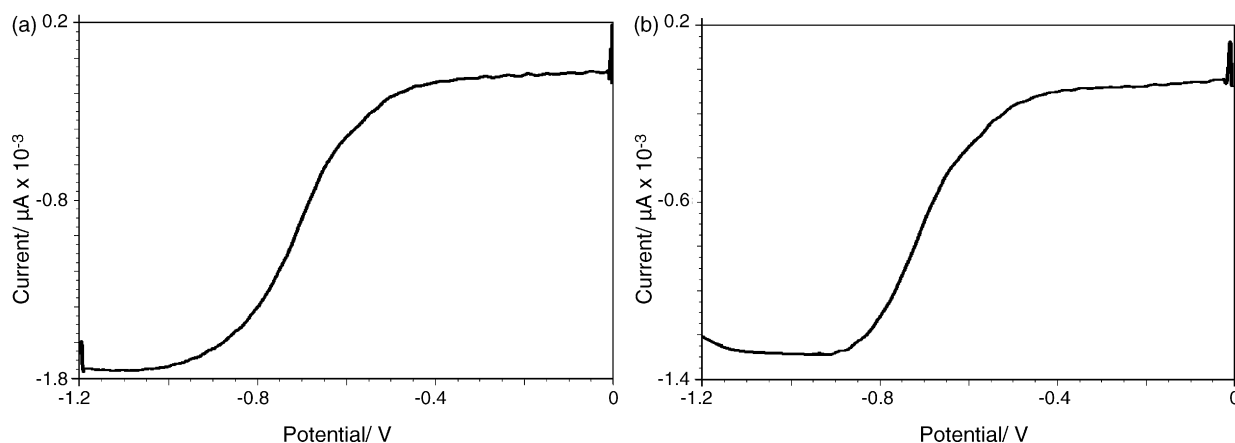


Fig. 6. UME curves of DMSO solutions of  $1.0 \times 10^{-5}$  M compounds **5b** (a); **7b** (b) in the presence of 0.1 M TBA<sup>+</sup>BF<sub>4</sub><sup>-</sup> at 10 μm-platinum ultramicro electrode. Potential scan rate: 10 mV s<sup>-1</sup>.

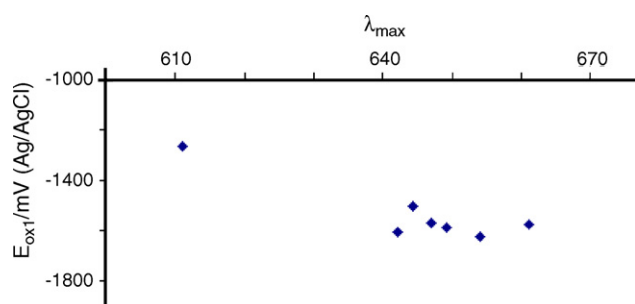


Fig. 7. The correlation between the  $\lambda_{\max}$  and the  $E_{\text{ox1}}$ /mV (Ag/AgCl) values.

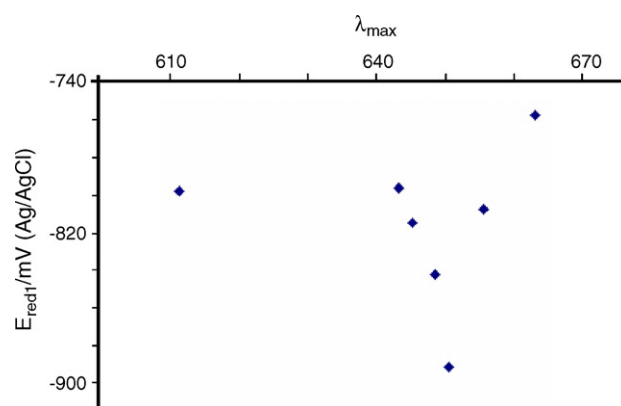


Fig. 8. The correlation between the  $\lambda_{\max}$  and the  $E_{\text{red1}}$ /mV (Ag/AgCl) values.

If  $i_t$  values are plotted against  $t^{-1/2}$  from the resulting slope  $n$  could easily be calculated. The number electrons calculated are given in Table 4.

As seen from Fig. 5 and Table 4, there is a one-electron transfer wave for Ni-TPF (**1b**). Ni-TPF (**1b**) is fragmented. Ni<sup>2+</sup> and formazan anion (TPF<sup>-</sup>, **X**) are formed in solution (Scheme 3). TPF<sup>-</sup> anion gives a single one-electron transfer giving a formazan radical (TPF<sup>•</sup>). These radicals give a disproportionation reaction to give a formazan (TPF) and tetrazolium cation (TPT<sup>+</sup>) or a dimerization reaction resulting a diformazan. Mechanism of the oxidation of compound **1b** is shown in Scheme 3. These results are in agreement with literature [15].

Both the nickel(II) complexes of -CH<sub>3</sub> and -OCH<sub>3</sub> substituted formazans gave clear S-shaped steady state currents with UME (Figs. 5 and 6). As seen from Fig. 5, there are one-electron transfer wave for compounds **2b** and **4b**. The numbers of electrons transferred are two for *o*-, *p*-CH<sub>3</sub> substituted nickel(II) complexes in UME based cyclic voltammograms of based UME and chronoamperometric (Table 4). This is accordance with CV results (Fig. 3). The appearance of one distinctive peak in *o*-, *p*-CH<sub>3</sub> substituted nickel(II) complexes suggest that the compounds give two-electron transfer. Complexes **2b** and **4b** give one-step

Table 5  
The total  $\sigma_T$  ( $\sigma_1 + \sigma_2$ ) and related  $\lambda_{\max}$  values

Substituent position	Compound	Abbreviation	$\sigma'$ (s)	$\sigma_T$ (total effect)	$\lambda_{\max1}$ (nm)
<i>m</i> -	<b>1b</b>	H	H: 0	0	611.0
	<b>3b</b>	<i>m</i> -CH <sub>3</sub> , <i>p</i> -OCH <sub>3</sub>	<i>m</i> -CH <sub>3</sub> : -0.06; <i>p</i> -OCH <sub>3</sub> : -0.12	-0.18	647.0
	<b>6b</b>	<i>m</i> -OCH <sub>3</sub> , <i>p</i> -OCH <sub>3</sub>	<i>m</i> -OCH <sub>3</sub> : 0.10; <i>p</i> -OCH <sub>3</sub> : -0.12	-0.02	649.0
<i>p</i> -	<b>4b</b>	<i>p</i> -CH <sub>3</sub> , <i>p</i> -OCH <sub>3</sub>	<i>p</i> -CH <sub>3</sub> : -0.14; <i>p</i> -OCH <sub>3</sub> : -0.12	-0.26	644.0
	<b>7b</b>	<i>p</i> -OCH <sub>3</sub> , <i>p</i> -OCH <sub>3</sub>	<i>p</i> -OCH <sub>3</sub> : -0.12; <i>p</i> -OCH <sub>3</sub> : -0.12	-0.24	642.0

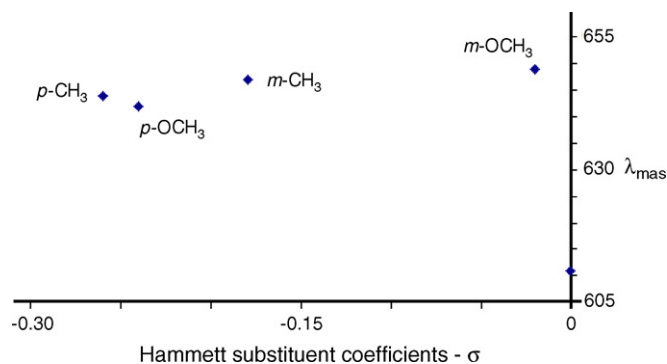


Fig. 9. The  $\lambda_{\max}$  values against Hammett substituents coefficients- $\sigma$ .

two-electron transfer giving directly tetrazolium cations. Mechanisms of the oxidation of compounds **2b** and **4b** are shown in Scheme 3b. These results are in agreement with the literature [16].

As seen from Figs. 5, there are one-electron transfer wave for compound **3b**. The number of electrons transferred is one for *m*-CH<sub>3</sub> substituted nickel(II) complexes cyclic voltammograms of based UME and chronoamperometric (Table 4). This is accordance with CV results (Fig. 3). The appearance of one distinctive peak in *m*-CH<sub>3</sub> substituted nickel(II) complex suggest that the compound gives one-electron transfer. This complex (**3b**) is fragmented. Ni<sup>2+</sup> and substituted formazan radicals are occurred in solution (Scheme 3a). These radicals give a disproportionation reaction to give a substituted formazan and tetrazolium cation or a dimerization reaction result a diformazan. Mechanism of the oxidation of *m*-CH<sub>3</sub> substituted nickel(II) complex (**3b**) is shown in Schemes 3a. These results are in agreement with the literature [15].

As seen from Fig. 6, there are one-electron transfer wave for compounds **5b–7b**. The numbers of electrons transferred are two for *o*-, *m*-, *p*-OCH<sub>3</sub> substituted nickel(II) complexes cyclic voltammograms of based UME and chronoamperometric (Table 4). This is accordance with CV results (Fig. 4). The appearance of one distinctive peak in *o*-, *m*-, *p*-OCH<sub>3</sub> substituted nickel(II) complexes suggest that the compounds give two-electron transfer. Complexes **5b–7b** give one-step two-electron transfer giving directly tetrazolium cations. Mechanisms of the oxidation of compounds **5b–7b** are shown in Scheme 3b. These results are in agreement with the literature [16].

#### 4. Conclusions

Nickel(II) complexes of formazan were synthesized. The products obtained were purified by repeated crystallization from methanol and the purity was checked by TLC. Spectroscopic characteristics of the prepared complexes are discussed. Determined peak potentials ( $E_{ox}$  and  $E_{red}$ ), diffusion coefficients, number of electrons transferred ( $n$ ) and heterogeneous rate constants ( $k_s$ ) were obtained with the use of cyclic voltammetry, linear sweep voltammetry and chronoamperometry. The oxidation products prepared by controlled potential electrolysis (CPE) were isolated and identified by different techniques: GC–mass and elemental analysis. The oxidation mechanism was occurred in a single step two-electron or one-electron transfer to a disproportionation or dimerization reactions following the radical formation step.

The spectral and redox properties were compared. There was a relatively good correlation between the  $\lambda_{max}$  and peak potentials ( $E_{ox1}$  and  $E_{red1}$  values) (Figs. 7 and 8).

It was also investigated whether the Hammett substituent coefficients could be used to evaluate the total effect of the two different substituents, upon the  $\lambda_{max}$  values and thus the color. Hammett substituent coefficients  $\sigma$  have been related with  $\lambda_{max}$  values for only one substituent in the structure up to now. The total  $\sigma_T$  ( $\sigma_1 + \sigma_2 = \sigma_T$ ) and related  $\lambda_{max}$  values are at Table 5.  $\lambda_{max}$  values have been correlated to Hammett substituent coefficients ( $\sigma_T$ ). Representative  $\lambda_{max}-\sigma_T$  plots are illustrated in Fig. 9.

There were linear correlation between Hammett substituent coefficients- $\sigma$  with  $\lambda_{max}$  values for the nickel(II) complexes.

#### Acknowledgement

We are very grateful to the Gazi University Research Fund for providing financial support for this Project (No. 04/2004-13).

#### References

- [1] J.W. Lewis, C. Sandorfy, Can. J. Chem. 61 (1983) 809.
- [2] A.R. Katritzky, S.A. Belyakov, D. Cheng, H.D. Durst, Synthesis 5 (1995) 577.
- [3] H. Tezcan, N. Ozkan, Dyes Pigments 56 (2003) 159.
- [4] H. Tezcan, T. Uyar, R. Tezcan, Turk. J. Spectrom. Aegean Univ. 10 (1989) 82.
- [5] W. Czajkowski, R. Stolarski, M. Szymczyk, G. Wrzeszcz, Dyes Pigments 47 (2000) 143.
- [6] Y. Gök, M. Tüfekci, E. Ozcan, Synth. React. Inorg. Met. –Org. Chem. 23 (1993) 861.
- [7] Y.M. Issa, M.S. Rizk, W.S. Taylor, M.H. Soliman, J. Indian Chem. Soc. 70 (1993) 5.
- [8] D.A. Brown, H. Bögge, G.N. Lipunova, A. Müller, W. Plass, K.G. Walsh, Inorg. Chim. Acta 280 (1998) 30.
- [9] A. Uchiumi, A. Takatsu, H. Tanaka, Anal. Sci. 7 (1991) 459.
- [10] Y. Kawamura, J. Yamauchi, H. Ohya-Nishiguchi, Bull. Chem. Soc. Jpn. 66 (1993) 3593.
- [11] M. Szymczyk, A. El-Shafei, H.S. Freeman, Dyes Pigments 71 (2006) 206.
- [12] V.C. Schiele, Ber. 30 (1964) 308.
- [13] A.M. Mattson, C.O. Jensen, R.A. Dutcher, Science 5 (1947) 294.
- [14] H. Wan, R. Williams, P. Doherty, D.F. Williams, J. Mater. Sci.: Mater. Med. 5 (1994) 154.
- [15] K. Umamoto, Bull. Chem. Soc. Jpn. 62 (1989) 3783.
- [16] G.M. Abou Elenien, J. Electroanal. Chem. 375 (1994) 301.
- [17] A.S. Baranski, W.R. Fawcett, C.M. Gilbert, Am. Chem. Soc. 57 (1) (1985) 166.
- [18] D.H. Williams, I. Fleming, Spectroscopic Methods in Organic Chemistry, McGraw-Hill Publishing Company Limited, London, 1966.
- [19] F. Schiman, Nuclear Magnetic Resonance of Complex Molecules, vol. 1, Vieweg and Sohn GmbH, Braunschweig, 1970.
- [20] L.J. Bellamy, The Infrared Spectra of Complex Molecules, Methuen, London, 1962.